Recent Developments in Biotransport[1]

Liang Zhu
Associate Professor of Mechanical Engineering
Department of Mechanical Engineering,
University of Maryland Baltimore County,
Baltimore, MD 21250
e-mail: zliang@umbc.edu

In the past ten years, one has seen rapid advancements in heat and mass transport applications in biology and medicine. The research activities have been shifted from fundamental development of better theoretical models accurately describing the thermal effect of local vasculature geometry and blood perfusion rate in the 1980s and 1990s to emphases on biotransport research with clear clinical applications and on how to utilize theoretical simulation and imaging techniques for better designing treatment protocols in those applications. This review will first describe briefly technical advancements in bioheat and mass transfer in the past several decades and then focus on two important applications in bioheat and mass transport covering different temperature ranges: hypothermia in brain injury and hyperthermia in tissue thermal damage. The contributions of nanotechnology, imaging tools, and multiscale modeling to the advancements will be discussed in the review. [DOI: 10.1115/1.4003511]

1 Introduction

Biotransport is an interdisciplinary research field applying traditional thermal and fluid principles to biology and medicine. Although studies of thermal properties and physics to understand biological processes such as thermoregulation and body's responses to harsh environments can be traced back to the 18th century, a systematic evaluation of biotransport occurred after Pennes' publication of his development of the Pennes bioheat equation and his experimental validation of this model [1]. It has been well known that the complicated vascular geometry and local blood perfusion variations and dynamics have profound thermal effects on local temperature distribution in human tissue. The simplification of these thermal effects to a single perfusion source term added to the traditional heat conduction equation in the Pennes bioheat equation has provided opportunity for engineers to predict tissue temperature fields with the available analytical solutions and numerical simulation techniques at that time.

Since the 1980s, the accuracy of the Pennes bioheat equation has been questioned by researchers, primarily the assumptions made when the equation was initially derived [2–4]. Later, experimental and theoretical studies provided direct evidence of precapillary arterioles as thermally significant blood vessels and important thermal contribution from countercurrent artery-vein pairs to the surrounding tissue, both of which were neglected in the Pennes bioheat equation [5–10]. Several continuum models were then developed to address the limitations of the Pennes bioheat equation in the 1980s and 1990s based on various vascular structures from one organ to another and from one layer to another [3,11–14]. Most of the continuum models rely on analyzing the thermal interaction between a representative tissue unit and a typical vasculature structure embedded in the unit. The averaged thermal effect from the analyses was used to evaluate the accuracy of the Pennes bioheat equation. One of the models is the Weinbaum–Jiji bioheat equation, which models the thermal effect of local blood perfusion as an enhancement in tissue thermal conductivity, mainly due to the significant contribution from countercurrent arterial and venous heat exchange.

Since both the Pennes and Weinbaum–Jiji models represent two extreme conditions of how to model the venous rewarming contribution in tissue-vessel thermal interaction, later studies have suggested that one way to overcome the limitations of both models is to introduce a "correction coefficient" to the Pennes perfusion source term. Typically, the strength of the perfusion term was derived from calculating the average heat released from a vascular network to a tissue unit. One early work [11] was based on a generated vascular network following diffusion of angiogenic factors in tissue. It has been shown that the Pennes perfusion source term overestimates the strength of heat released to or absorbed by the local blood perfusion by approximately 20%. Another study [13,14] simulated the temperature field of thermally significant countercurrent artery and vein pairs embedded in repetitive tissue cylinders in muscle tissue. The anatomic data of the vascular arrangements of various skeletal muscles have led to calculations of correction coefficients of 0.6–0.8, suggesting 20–40% of venous rewarming and implying a significant overestimate of the thermal effect by the Pennes perfusion term in muscle tissue. The accuracy of the calculated correction coefficients in the previous studies still depends on the precise description of the local vasculature arrangements and whether a repeatable tissue unit can be identified in the targeted tissue region. Unfortunately, in the tissue region such as tumors, the blood flow patterns are often irregular and unpredictable, making the derivation of the correction coefficient a difficult task. There were only a few attempts to develop alternative bioheat transfer models in the past ten years based on volume averaging temperatures of porous media [15,16]. One thing that is not clear from those models is the calculation of the "to-be-determined" parameters appearing in those equations. The determination of those parameters still requires a development of a vasculature-tissue unit for establishing their relationship to the specific vasculature and blood perfusion rate.

Although developments of new bioheat transfer models have attracted a lot of attention in the 1980s and 1990s, most of the developed bioheat models have not yet been applied regularly by bioengineering researchers due to the uncertainty of estimating the parameters such as the enhancement in tissue thermal conductivity and the correction coefficient. The Pennes bioheat equation, utilizing only local perfusion rate and arterial blood temperature, is relatively easy to use without detailed anatomic knowledge of their vasculature. In the past 10 years, very limited efforts have been focused on developing a better bioheat transfer model, with a few exceptions [15,16]. Currently, the thermal effects of small blood vessels are still normally modeled by the Pennes perfusion source term, with special treatments to the large vessels. The emphases of bioheat transfer modeling have been shifted to model large individual blood vessels and its thermal interaction with the detailed anatomic geometry in the tissue region. This is largely

[1]Invited paper.

Contributed by the Heat Transfer Division of ASME for publication in the JOURNAL OF THERMAL SCIENCE AND ENGINEERING APPLICATIONS. Manuscript received November 24, 2010; final manuscript received January 4, 2011; published online February 24, 2011. Assoc. Editor: Lisa X. Xu.

due to the advancements in computational resources, which allow import of three-dimensional tissue geometry from magnetic resonance imaging (MRI) or computer tomography (CT) imaging systems to commercially available numerical simulation software packages. The dramatic increase in computer memory and calculating speed in the past decade enables the simulation of both steady state and transient temperature distribution in three-dimensional tissue structures with embedded individual large blood vessels.

In the past decade, four research areas in bioheat and mass transport have attracted a lot of attention from biomedical engineering researchers. Each addresses a specific temperature range: cryosurgery and cryopreservation, brain hypothermia for cerebral injury, hyperthermia in tissue thermal damage, and tissue ablation in surgical procedures or accidental tissue burning. Manipulating various strategies, including cooling rate, cooling temperature, chemical additive, etc., to achieve preferred cooling mechanisms such as vitrification has shown great progress in cryopreservation in the past several decades to minimize chemically driven deterioration processes due to ice formation within and between cells. A detailed review in cryosurgery and cryopreservation has been done by Bischof [17], Diller [18], and others. On the other hand, tissue ablation due to exposure to extremely high temperature sources such as laser and fire for an extended period of time requires a fundamental understanding of thermal burning processes involving not only temperature elevation distribution, but also biochemical reaction to the extreme temperature rises (heat shock proteins), as well as mechanical destruction (vaporization and acoustic waves) and removal of the tissue. Those multiple mechanisms have added challenges to bioengineers since tissue damage may not be due to thermal effect alone. Experimental studies in this area have provided insights on the contributions of individual mechanisms and processes. Developing realistic models to predict thermal, biochemical, and mechanical processes during high temperature exposures has led to alternative burning simulations or thermal ablation protocol optimizations, therefore minimizing unnecessary animal and human experiments, which are often difficult to conduct. Several excellent reviews in this topic can be found in the review papers by Diller [18,19], and laser induced tissue ablation is well described in a book edited by Welch and van Gemert [20]. In this paper, we will focus our review on the other two bioheat and mass transport topics: hypothermia in cerebral injury and hyperthermia in tissue thermal damage. Brain hypothermia involves brain temperature reduction of several °C below normal tissue temperature, while hyperthermia treatment for killing cancer cells requires temperature elevations of at least 6°C above 37°C for a long duration from minutes to hours. Although both topics are not new, we have seen technical advancements contributed by bioengineers to use improved instrumentations to measure and observe thermal property responses to heating or cooling, to simulate thermal and mass transport processes during the therapy, to design an effective system for delivering thermal dose to targeted areas, and to develop optimized treatment plans for improving efficacy and safety. The newly developed imaging tools, nanotechnology, and advanced multiscale modeling approach will be discussed in the review.

2 Hypothermia for Neuroprotection

Hypothermia in brain tissue has been demonstrated as an effective therapeutic adjuvant for brain tissue damage due to traumatic brain injury, stroke, cardiac arrest, etc. The animal and clinical results in the past several decades have suggested that mild hypothermia with a temperature reduction of a few °C improves patients' outcomes while minimizing systemic complications associated with deep or moderate hypothermia. Cooling initiation before or after injury, cooling duration, cooling extent, and rewarming rate are important factors, which may affect the neuroprotection of the cooling approach. Currently, there are still opportunities for engineers to design clinically feasible cooling devices or approaches and use theoretical simulations to optimize cooling protocols for improving treatment efficacy.

2.1 Efficacy of Hypothermia in Improving Patients' Outcome. Early animal and clinical studies for cardiac arrest patients from the 1940s to 1960s have suggested longer brain tolerant time to brain ischemia or cardiac arrest than that during normothermic conditions [21–24]. Many of the surgical procedures require the surgeon to work with a bloodless field, which often leads to temporary brain ischemia. It has been shown that inducing hypothermia in heart and/or brain tissue in conjunction with those surgical procedures would result in less permanent brain damage after surgically induced brain ischemia. The surgical interruption time can be implemented for more than 45 min when the brain tissue is maintained at 10°C versus only 8 min at 32°C in brain tissue. Hypothermia significantly improved the ability of surgeons in working with previously inoperable cardiac and cerebral diseases and reduced patients' mortality.

Hypothermia applications suffered a setback in the 1970s due to bad management of cooling extent and systemic complications. Mild hypothermia (34–36°C) has been attracting attention since the 1980s due to encouraging animal experiments on canine, swine, and rodent models when systemic complications were minimized during mild hypothermia procedures [25]. Animal studies allow extensive and controlled experiments to evaluate the effect of various factors such as cooling methods, temperature depression, hypothermia duration, cooling initiation relative to the ischemic event, and rewarming rate on the brain recovery from ischemia. Evidence is strong to support hypothermia induced neuroprotection from ischemia injury in laboratory animals [26]. It has been suggested that early cooling initiation before or right after brain injury is a key to yield meaningful neuroprotection in those studies [27,28]. Therefore, it is not a surprise to see more success in controlled applications, such as multiple scleroses (MS) and open heart and neck surgery, than that in traumatic head injury when the time to initiate cooling is typically several hours after the injury. Nevertheless, delayed cooling initiation may still be compensated by prolonged cooling durations and/or controlled cooling temperature and slow rewarming rate.

2.2 Hypothermia Approaches. Two potential neurological damages require whole body cooling to control the body core temperature. One is during heat stroke when the body temperature is elevated above 37°C due to dysfunction and/or failure of temperature control in the human body. It occurs when the body is exposed to hot weather with high humidity and/or during strenuous exercise. Sport-related deaths due to high temperature environment during exercise have been reported. In the U.S., there are more than 300 heat stroke–related deaths each year. The other group sensitive to body temperature elevations is the group of MS patients. Their symptoms tend to get worse when the body temperature is even slightly elevated. Although exercise is beneficial to those patients physically and physiologically, exercise induced body temperature rise will exacerbate MS symptoms.

Typical cooling approaches to lower the body temperature include immersing the body in cold water (bathtub, swimming pool, river, etc.), wearing a light weight cooling jacket, enhancing heat dissipation via convection and/or evaporation, etc. Most of the approaches cool down the body slowly due to the large body mass; however, a body temperature reduction or maintenance of a normal body temperature can still be evident if the method is implemented for a period of time (approximately in hours). Studies have shown that cooling may restore neuronal activities, which lead to proliferation, migration, and maturation of myelin producing cells in MS patients [29,30]. Improved physical strength and visual acuity and minimization of tremor and pain have been reported in MS patients with controlled body temperatures [31]. In sport medicine, trainers have utilized a hand cooling device to counteract the temperature elevations during strenuous physical

training. This approach takes advantages of the rich arteriovenous anastomoses (AVAs) in the hand region. The hand is inserted into an apparatus that can induce negative pressure and also serve as a cooling device. Applying negative pressure to the hand would open up the AVAs and divert a large portion of the cardiac output to the hand where the cooling device is placed. Experimental studies on healthy athletes have shown substantial normal body temperature control by implementing the hand cooling device compared with the group without the device during sport training [32–34]. Temperatures of the body core have been shown to drop from 39 °C back to 37 °C within 15 min by the approach during a heavy exercise. In principle, this method should also be applied to achieve fast cooling in brain injury patients. However, physicians have cautioned the danger of a sudden blood pressure drop due to a large amount of blood diverted to the hand. For patients with compromised health, the body may not be able to respond quickly to the pressure drop by adjusting other circulation parameters as healthy athletes.

For patients suffering neurological ischemic injury, such as stroke, traumatic brain injury, and spinal cord damage, the previously mentioned whole body cooling approaches are still useful to cool the brain tissue. The drawbacks are slow cooling rates due to the large body mass [35–37]. To address this limitation, an endovascular cooling device has been developed to lower the temperature of the cardiac output quickly. A catheter is inserted into the femoral vein, and heat is carried out from the warm venous blood by the circulating coolant. This method is very effective to induce several °C temperature reduction of the body within 10–20 min [38–40]. However, it involves relatively invasive procedures and requires intensive medical support and a skillful surgeon to implement the approach. In addition, systemic complications due to the induced moderate hypothermia in the entire body may counteract the neuroprotection of cooling and affect the patients' recovery. Randomized clinical studies using large sample sizes are still needed to evaluate the long term safety and efficacy of this approach.

For brain injury patients, it is the brain tissue that needs to be cooled to improve patients' outcomes. Cooling the entire body to achieve a temperature reduction in the brain may not be necessary since the human brain represents only 2% of body mass. In recent years, selective brain cooling (SBC) in which the brain temperature is reduced while the rest of the body is kept normothermia has been proposed to minimize serious adverse systemic complications. Simple selective brain cooling approaches may also maximize the protective benefits of hypothermia if it can be initiated by emergency medical services (EMS) personnel during the transportation of the patients to the hospital. The brain tissue can be directly cooled using a cooling helmet or via infusing chilled saline to the cortex surface or inserting an intraparenchymal cooling catheter. However, limited cooling penetration through the scalp and skull and the high metabolism in the brain tissue typically confine the temperature reduction in the brain superficial region such as the cortex or in the region surrounding the cooling probe [41–46]. Vasoconstriction in the scalp, shivering, and nonuniform temperature fields in the brain tissue are some of the drawbacks associated with scalp surface cooling.

On the other hand, cooling the blood supplied to the brain tissue may result in very uniform temperature reductions in the brain tissue due to the large local blood perfusion rate in the brain. This approach also bypasses the skin since the cooling is from the inside of the brain tissue. Shivering driven by skin receptors would be unlikely. In recent years, it is proposed to insert a cooling catheter into the femoral vein and advance it to the common carotid artery to achieve rapid cooling of the arterial blood. Self-sustained coolant can be circulating within the catheter without physical contact with the blood. Cold saline can be infused to mix with the carotid arterial blood to induce moderate brain hypothermia within a few minutes [47,48]. The technical challenge is the invasive nature of this approach. Antithrombotic coating is needed to prevent clotting in the carotid artery. Increases in arterial pressure due to saline infusion may also cause some complications to patients with compromised health.

Another blood cooling technique via inserting a cooling device through the neck muscle and placing the device on the carotid artery surface has been proposed to achieve temperature reductions of several °C within 30 min [49–51]. Theoretical simulation and experiments performed in a tissue equivalent gel have shown the targeted temperature reduction if good physical contact between the device and the artery is ensured [52]. In addition, this method may be more suitable for applications when the carotid artery has to be exposed, therefore minimizing any additional physical manipulation of the sensitive region surrounding the carotid artery.

Neck collars have also been suggested to cool the arterial blood supply. The portable nature and compact size of the collar may shorten the time duration between brain injury and cooling initiation to confer neuroprotection to the patients. However, previous theoretical simulations have suggested very limited temperature reductions along the carotid arteries and vertebrate arteries (<0.5 °C) even when the neck surface temperature is reduced to 0 °C [53,54]. This is largely due to the thick neck muscle that presents a large conduction resistance to yield very limited cooling penetration to reach the arterial blood. On the other hand, neck collars may be suitable to achieve meaningful cooling to the superficial jugular veins to prevent body temperature elevations for conditions such as hot weather and/or exercise [54].

2.3 Engineer Contribution to Hypothermia. Engineers can contribute to brain hypothermia studies via designing effective and safe cooling devices. Currently, there are primarily two kinds of cooling equipment for body and brain hypothermia. One is to cool the targeted tissue via the body surface. Most of them are simple cooling vests, helmets, and pads, which do not require sophisticated control units. Engineers design those cooling equipment to achieve targeted temperature reductions on the body surface. This typically can be achieved via testing different cooling contact surfaces, selecting an appropriate coolant, and evaluating thermal properties of the material in contact with the body, estimating heat exchange with the environment from the coolant reservoir and the entrance of cooling devices, etc. Patient's safety issues, including vasoconstriction, shivering, freezing damage to skin surface, and possible interference with the medical treatment equipment, should also be taken into consideration since they may affect the cooling efficacy and feasibility of implementing the cooling devices.

The other kind of cooling equipment consists of endovascular cooling catheters for inducing fast cooling in the body. There are engineering aspects in designing the device for size minimization with targeted cooling capacity. The catheter diameter needs to be smaller than 5 mm to be inserted into the femoral vessels. Coolant is self-contained so that coolant channels are embedded inside the small catheter. The material of the catheter and its embedded inner structure needs to be flexible for navigating inside the blood vessels. FDA approval is required for those endovascular cooling devices concerning patient safety. For example, the catheter may cause clotting if the surface is not coated properly by antithrombotic agent [55]. Selecting a proper coolant is also important in the case of leakage. It needs to be kept in mind that endovascular cooling is used adjunctive to other routine medical treatments. Therefore, the modified procedures to accommodate the cooling methods should not be too invasively aggressive to interfere with the major therapeutic procedures. Sometimes this may require sacrifice of some cooling capacity for the safety of the patients.

In recent years, theoretical modeling of the temperature fields in the spinal and head regions has been used not only to illustrate the possible cooling extent in those targeted regions, but also to help design effective and safe hypothermia therapy [56–60]. Theoretical simulation addresses the difficulty of inserting too many temperature sensors in the brain tissue during the therapy, as well as

poor spatial and temporal resolutions and high operating costs of noninvasive temperature monitoring systems such as MRI. Another advantage of theoretical modeling is to identify tissue locations, which are critical to monitor the cooling extent and to assess patient safety. The vast data resulted from parametric studies provide insight on how the large variations of geometrical and physiological parameters affect the efficacy of hypothermia therapy. Therefore, the treatment protocol and device design may be optimized to address the uncertainty associated with individual patients.

Most of the theoretical simulations use the Pennes bioheat equation to model the thermal contribution of local vascular geometry and blood perfusion rate to the local tissue temperature field. During hypothermia, tissue temperatures are typically lower than the arterial blood temperature, implying that local blood perfusion (ω) serves as heat sinks in the tissue. Based on the Pennes perfusion heat source/sink term, the strength of the heat sinks is directly proportional to the local blood perfusion rate. Therefore, it is a challenge to cool highly perfused tissue regions such as brain and spinal cord since the penetration of cooling from the cooling device is facing the fast refreshing of warm arterial blood in those tissue regions, resulting in a shallow cooling penetration. Previous theoretical studies have shown a penetration depth of only 10 mm in the brain gray matter. However, ischemia in brain and spinal cord due to injury or temperature reduction actually promotes cooling penetration to a large injured area. It can be concluded that the penetration depth (d) is approximately inversely proportional to the square root of the blood perfusion rate, i.e., $d \propto \omega^{-1/2}$ [46]. Therefore, the covered cooling area can be doubled in distance from the cooling front when the local blood perfusion rate decreases to one-fourth of its normal value. For an injured brain gray matter, the cooling penetration can be extended to 20 mm when the blood perfusion rate is markedly reduced from 80 ml/min 100 g tissue under normal conditions to 20 ml/min 100 g tissue after injury [46].

There are several attempts to model individual blood vessels in the tissue regions. Typically, it is used in hypothermia approaches involving carotid arterial and jugular venous cooling, where point-to-point simulations along those large blood vessels are necessary. Due to the complexity of the vasculatures, the vessels are modeled as straight tubes without considering vessel bifurcation and tapering geometry [49,53,54]. The simulation results are relatively accurate since the temperature reduction along those vessels is largely determined by the blood flow rate in the vessels and local geometrical variation plays a very minor role in the blood cooling.

Recent advancements in computational resources have provided the possibility in developing accurate theoretical models for hypothermia therapy. Imaging technologies such as MRI can scan the detailed individual structures in the head regions. Commercially available numerical simulation software packages allow import of the 3D geometry into grid-generation algorithms for temperature simulations [56,58]. Inclusions of additional details of the brain geometry and vasculature into the theoretical model would further improve the predictive capability of the simulations.

One challenge in theoretical simulation is how to assess local blood perfusion responses to cooling. In most previous theoretical studies, the blood perfusion rate is either considered as a constant or assumed to decrease with temperature reductions. However, as shown in an in vivo animal study [61], all the animal subjects during head surface cooling showed a changed blood flow rate in the common carotid artery, an index of the global blood perfusion rate in the brain. To further complicate theoretical analyses, the reduction in the blood flow rate in the common carotid artery did not have the same pace, varying from 5 min to more than 40 min to establish a steady state during the cooling. The relationship between local blood perfusion rate and temperature reduction has been proposed to follow the Q_{10} law, representing a linear relationship between $1/T$, where T is the tissue temperature, and log $CMRO_2$ (oxygen consumption rate) [62]. This relationship is indeed derived from experimental measurements. However, extrapolating it to the cooling response of local blood perfusion rate has implied that local blood perfusion rate and oxygen consumption rate are coupled, which may be true under normal conditions. After brain ischemia injury, the local blood perfusion rate may be decoupled from the local metabolic rate (oxygen consumption rate). The laser Doppler flowmeter (LDF) method is normally used to assess changes in local blood perfusion rate on the brain surface. Most of the LDF measurements have suggested blood perfusion reduction of cerebral cortex; however, an increase in the blood perfusion rate after brain ischemic damage has also been reported. Using a colored microsphere technique further demonstrated nonuniform blood perfusion responses from one brain region to another. Further, it is uncertain whether the measured blood perfusion responses in animal models are applicable to humans due to the geometrical difference and tolerance to cooling. Three-dimensional MRI scanning may be a suitable alternative to monitor the blood perfusion changes during cooling when it becomes a routine assessment tool with affordable expenses when used in clinical studies. Currently, the uncertainty of the blood perfusion rate in the targeted region will continue to complicate theoretical predictions.

3 Hyperthermia in Tissue Thermal Damage

Within the past three decades, hyperthermia has been evaluated in a variety of therapeutic procedures for killing tumor cells in cancer treatment. It is preferable for patients diagnosed with previously inoperable or surgically complex tumors or for patients looking for an alternative to costly and risky surgical procedures. In hyperthermia, thermal energy delivered to tumors raises the entire tumor temperature field above 43 °C for durations of more than 60 min while maintaining the temperatures in the surrounding normal tissue below 43 °C. It has been suggested that either temperature elevations produce a thermal induced cytotoxic response or temperature rises enhance the cytotoxic effects of radiation and drugs. Both the direct cell-killing effects of heat and the sensitization to other agents by heat are phenomena strongly dependent on the achieved distribution of the temperature increases and the duration of heating in tumors.

3.1 Traditional Hyperthermia Approaches. Earlier hyperthermia approaches in the 1980s and 1990s include high energy dc shock (electric conductive heating), radio frequency (alternating current), microwave (electromagnetic wave absorption), laser, etc. All the methods require either a wave or a current passing through the tissue and its interaction with molecules in the tissue to generate heating. The wave or current decays as it passes through the tissue, resulting in a heating density diverging from the location where the wave or current is initiated. Collateral thermal damage to healthy tissue may occur if the targeted tissue region is not located very close to the initiation. Actively cooling the healthy tissue region has been shown to be effective to minimize undesired thermal damage.

In electric cardioversion, synchronized high energy dc shock is used for the treatment of tachycardia and arrhythmias to correct abnormal heart rhythms and to restore normal sinus rhythm. However, due to the very large voltage and current involved in the procedures, a very high temperature at the electrode surface may induce localized tissue ablation [63]. Complications such as explosive gas formation and shock wave may occur.

Radio frequency waves typically have an alternating current at a frequency of 200–1000 kHz. Similar to a dc shock, two electrodes are needed and local temperature elevations are due to ohmic heating. Since the current is inversely proportional to the square of the distance from the electrode surface, overheating in a narrow region close to the electrode may be inevitable [64–67].

Microwave heating utilizes electromagnetic wave at a frequency of megahertz or gigahertz, which travels through cables and radiates to tissue through a small antenna. Unlike radio fre-

quency heating, the heating mechanism is through interactions between the propagating electromagnetic wave and dielectric molecules in the tissue. The collision between the energized dipole molecules to maintain alignment with the alternating electromagnetic field results in converting electromagnetic energy to heat. One of the limitations of microwave heating is its shallow penetration depth from the antenna. For biological tissue consisting of mostly water, the penetration is limited to 10–20 mm. Microwave heating has been used in treatments for prostatic tumor or benign prostatic hyperplasia (BPH) (enlarged prostate) since the microwave catheter can be inserted through the urethra and advanced to the prostatic urethra close to the targeted prostatic tissue [68]. Cooling at the prostatic urethra using cold water has been shown to be effective to shift the maximal temperature location from the prostatic urethral surface to the transitional zone of the prostate.

Laser is a monochromatic electromagnetic wave, except that its wavelength is much shorter than that of microwave or radio frequency. Typical laser power level is less than 1 W; however, all the energy is concentrated on a very small tissue area of radius as small as 50 μm, resulting in highly concentrated temperature elevations. Laser wave can penetrate into tissue, and the resulting heat generation by tissue is due to laser energy scattering and absorption. The absorption and scattering of laser depend on both the tissue type (hard or soft) and the laser wavelength.

In the three primary clinical applications using laser, dermatologists and ophthalmologists are mostly using laser for blood vessel coagulation, and dentists use lasers in both soft and hard tissue ablation. The selection of laser type is largely determined by how deep the targeted region is located in the tissue. Typically, longer wavelength lasers penetrate more deeply into tissue than short wavelength lasers. One example is in laser coagulation of blood vessels in the eyes. Lasers can penetrate the vitreous easily with only minor absorptions ($\sim$5%) and reach the retina. Conventional treatment for superficial retinal arteries and veins utilizes short wavelength lasers such as argon laser (527 nm). It will not be suitable for treating deep choroidal feeder vessels [69]. Laser energy must penetrate the overlying retinal layer, retinal pigment epithelium (RPE), and choriocapillaries to reach the targeted choroidal feeder vessels. Previous experimental and theoretical studies have suggested using a near-infrared (NIR) laser such as a diode laser at 805 nm wavelength to deliver sufficient laser energy to the choroidal feeder vessels with minimal concomitant retinal and choroidal damage, especially to the sensitive RPE layer [69,70].

Similar approaches can be seen in using laser for the treatment of port wine stains (PWS), birthmarks due to deep dilated capillaries located superficially in the skin [71]. The absorption of laser occurs largely due to oxyhemoglobins (HbO_2) and deoxyhemoglobins (Hb) in the blood stream. Short wavelength lasers, such as pulsed dye lasers (PDLs) at 577 nm and 595 nm and potassium titanyl phosphate (KTP) laser at 532 nm strongly absorbed by both oxyhemoglobin and deoxyhemoglobin, have been shown to be effective in obliterating the blood vessels to improve the skin tone in PWS located less than 1 mm beneath the skin surface [72,73]. However, for deeply seated PWS, it has been proposed to use an Alexandrite 755 nm laser or a neodymium doped yttrium aluminum garnet (Nd:YAG) laser at 1064 nm, which can penetrate into several millimeters in skin tissue. In addition, coagulation of venous blood with rich deoxyhemoglobins is preferred to use Alexandrite laser since the absorption by Hb at 755 nm wavelength is stronger than the absorption by HbO_2. On the other hand, the Nd:YAG laser at 1064 nm is better for obliteration of arterioles since it is absorbed more by HbO_2 than by Hb. In recent years, it has been proposed to use a dual laser system (short and long wavelength lasers) targeting both superficial and deep blood vessels in a combined approach [74]. Thermal damage to the epidermis ($\sim$60 μm in thickness) may occur even with limited laser energy absorption there. One approach to minimize the thermal damage in epidermis is to use cryogen sprayed on the skin surface before or during laser treatment. Theoretical simulations have been performed to identify suitable cooling parameters for preventing collateral thermal damage while delivering sufficient laser energy to the targeted blood vessels located in the dermis.

In dentistry, both short wavelength lasers such as Nd:YAG, argon, and diode lasers and long wavelength erbium: yttrium aluminum garnet (Er:YAG) and erbium, chromium: yttrium, scandium, gallium, garnet (Er,Cr:YSGG) are used in cutting hard tissue, reshaping gums and implants, and removing debris. Recently, bacterial disinfection in deep dentin area using Er,Cr:YSGG lasers has been proposed for root canal procedures [75]. In addition, simple red lasers at 695 nm emitted from a small probe have been used for the diagnosis of caries hidden inside the teeth [76,77]. Comparing to dermatology and ophthalmology, there are relatively limited studies in dentistry to optimize treatment efficacy when selecting from a variety of lasers. There are also only a few studies to evaluate collateral thermal damages to the tissue surrounding the targeted tooth region.

3.2 Nanotechnology in Hyperthermia Treatment. Currently, two nanotechnologies have emerged as promising hyperthermia therapies due to their ability to confine adequate thermal energy in tumors. Both overcome the limitations of traditional hyperthermia approaches such as microwave and radio frequencies, which have short penetration depths into tissue and often cause collateral thermal damage to the superficial tissue layers. One uses magnetic nanoparticles to generate heat when the nanoparticles are subject to an alternating magnetic field. The magnetic field is usually generated by a coil with strong alternating electric currents passing through. Previous studies have shown that the magnetic field should be at least 2 kA/m to induce sufficient temperature elevations in tissue [78–83]. The system typically requires at least several kilowatts of power, and only a very small percentage ($\sim$10 W) is used to generate the heat by the magnetic nanoparticles.

Gold nanoshells or nanorods are newly developed nanotechnology and have been tested in the past several years in cancer treatment. Gold nanoshells consist of a solid dielectric nanoparticle core ($\sim$100 nm) coated by a thin gold shell ($\sim$10 nm). Gold nanorods have a diameter of $\sim$10 nm and an aspect ratio of approximately 4. Nanorods may be taken up by tumors more readily due to their smaller size than nanoshells. By varying the geometric ratio, the nanostructures can be tuned to have strong absorption and scattering to a specific laser wavelength. The enhancement in laser energy absorption is several orders of magnitude higher than that of traditional dyes, such as indocynine green dye [84]. Among a wide range of laser wavelengths, the NIR laser at $\sim$800 nm is the most attractive wavelength range to clinicians due to its deep optical penetration in tissue. For example, the attenuation coefficient of a laser at 800 nm is approximately 0.1 cm^{-1}, which is equivalent to a laser penetration of 10 cm in tissue. Therefore, the tissue would appear almost "transparent" to the 800 nm laser light before the laser reaches the nanostructures in tumors, with minimal laser energy wasted by the tissue without the nanostructures. The laser energy absorbed in an area congregating by the nanostructures is transferred to the surrounding tissue by heat conduction. As for a very deep-seated tumor, optical fibers have been proposed via minimally invasive surgery to bring the laser to the surface of the tumor. This approach not only achieves targeted delivery of laser energy to the tumor, but also maximally concentrates a majority of the laser energy to the tumor region.

Another advantage of the nanotechnologies is the ability to design optimized treatment protocols via using multiple intratumoral nanofluid injection sites to generate sufficient temperature elevations in the entire tumor. This strategy [83] offers the maneuverability to control nanostructure distribution in tumors with various sizes, shapes, and blood perfusion rates through manipulating the location of the injection sites and injection parameters. As illustrated in Fig. 1(*a*), a single injection site that is used in most of the

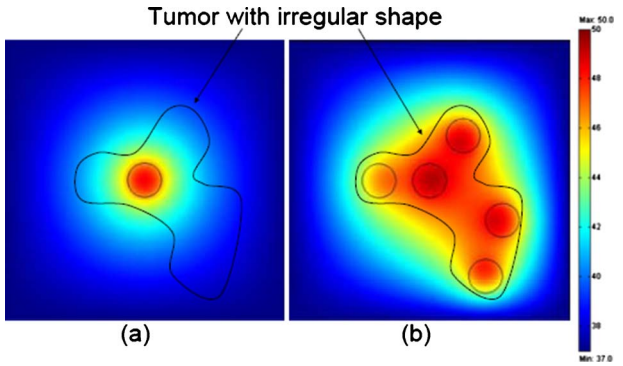

Fig. 1 Temperature elevations in a tumor with an irregular shape: (*a*) single injection and (*b*) multiple injections. Temperature elevations in the tumor are more uniform in (*b*).

current experiments causes localized heating resulting in underheating in the tumor periphery and/or overheating in the healthy tissue when the tumor has an irregular shape. Figure 1(*b*) demonstrates that temperature elevations can be nearly uniform throughout the entire tumor by using multiple injections of nanostructure deposition. The challenge in multisite injections is the design of an injection strategy addressing injection rate and amount and arrangement of injection sites that can lead to a sufficient and nearly uniform temperature elevation. This approach is unlikely to be affected by the high hydrostatic pressure in tumors since nanostructure deposition in the entire tumor is not necessary.

3.3 Progress in Magnetic Nanoparticle Hyperthermia for Cancer Treatment. Although magnetic nanoparticle hyperthermia was developed in the 1950s [85], it is still at an early stage of development in the treatment for malignant tumors. The heat generated by these particles when exposed to an external alternating magnetic field is mainly due to the Néel relaxation and/or Brownian motion of the particles [86,87]. Previous studies [88] showed that iron oxides magnetite Fe_3O_4 and maghemite γ-Fe_2O_3 nanoparticles are biocompatible to human tissue [87]. This method enables adequate heat to be generated within the tumor tissue without necessitating heat penetration through the skin surface, thus eliminating the consequent side effects of excessive collateral thermal damage. Magnetic nanoparticle hyperthermia has the versatility in treating deep-seated/irregular shaped tumors. Depending on the amplitude of the magnetic field and the particle size, the rate of temperature increase at the monitored site can be as high as several °C/min. Temperatures up to 71°C were recorded at the tumor center [87]. All the experimental data have suggested the feasibility of elevating the tumor temperatures to a level sufficient to kill tumor cells [80,88–94].

The employment of nanoparticles smaller than 100 nm is especially advantageous in generating sufficient heat with low magnetic field strength. The heat generated by magnetic particles subject to an alternative magnetic field is suggested to be primarily size-dependent. As the particle size decreases, thermal activation of re-orientation processes leads to a superparamagnetic (SPM) behavior that is capable of generating impressive levels of heating at low field strengths [95]. Spherical nanoparticles of 10 nm diameter are capable of providing a specific loss power (SLP) of 211 W/g under a magnetic field of 14 kA/m in amplitude and 300 kHz in frequency, whereas particles with a diameter of 220 nm only achieve a SLP of 144 W/g under identical magnetic fields. The application of nanoparticles in magnetic hyperthermia offers a more effective treatment route than microparticles.

Magnetic nanoparticle hyperthermia has been used to treat tumors in liver, kidney, and breast tissue. The particles used in previous studies included iron and iron oxide, while the iron oxides magnetite Fe_3O_4 and maghemite γ-Fe_2O_3 are the most studied to date. The reported magnetic frequency varied from 63 kHz to 700 kHz, while the lower and upper limits of the magnetic field strength were 2 kA/m and 24.8 kA/m. Particle sizes used are all smaller than 15 nm in diameter. The wide range of the reported specific absorption rate (SAR) measurements (28–467 W/kg) may be mainly due to the variation in magnetic field strength and frequency, nanoparticle concentration, and injection amount. For example, using an injected amount of nanofluid varying from 0.2 ml to 15 ml to tumor, Johannsen et al. [92,93] performed in vivo experiments of magnetic nanoparticle hyperthermia on human subjects in combination with external radiation. This combined treatment was found to reduce tumor growth by approximately 88% with a maximum and a minimum temperature of 58°C and 42°C, respectively. With a few exceptions, most of the experimental data are based on temperature measurements at one or two tumor locations. Later histological analyses have suggested underdosage heating (temperature increase lower than a critical value) in some tumor regions, usually at the tumor periphery.

3.4 Recent Experimental and Theoretical Investigations in Laser Photothermal Therapy. In the past several years, gold nanoshells, nanohorns, and nanorods have been developed as effective photo-absorbers in laser photothermal therapy in cancer research, similar to the concept of using indocyanine gree (ICG) dye [96] in the bloodstream to enhance laser absorption. Gold particles are biocompatible to tissue, and they allow conjugation of biomolecules to the gold surface. This method, if successful, would provide a powerful approach to concentrate laser energy in the tumor site and, therefore, to facilitate confined hyperthermia in tumors. The strong absorption is due to the optical resonances of gold when its size is much smaller than the visible light wavelength [97]. Laser light activates the electrons in gold, and when the electrons go back to its resting state, energy is released in the form of heat.

The feasibility of using laser photothermal therapy for tumor destruction has been tested both in tissue culture [98–103] and in implanted tumors in mice [97,104,105]. Most in vivo experiments performed on mice involve injecting approximately 0.1–0.2 ml nanoshell solution (concentration varies from 10^9 to 10^{11} nanoshells/ml solution). Since all implanted tumors are located superficially beneath the skin surface, it is expected that the laser energy is absorbed by the nanoshells accumulating in the tumor. Typical laser radiance at the surface is $2-50$ W/cm^2 for the photothermal therapy to be effective [99,104–107]. Laser spot size should affect primarily the affected tumor region laterally, and it varies from 1 mm to 5 mm [106]. Heating duration can be shorter than several minutes or longer than 15 min [101,106]. Successful treatments are illustrated by the shrinkage of the tumor following the laser therapy, as well as observed tumor cell death in the tissue culture [108]. Some experiments also measured temperatures at one or two tumor locations on the bottom of the tumor and found that the temperature rise and tumor shrinkage are also dependent on the concentration of the nanoshell solution [105].

Wide variation ranges of treatment protocols have been noted in previous experimental studies. For example, the nanoshell concentration in terms of numbers of particles (NPS) per unit volume before the injection varied from 10^9 NPS/ml to 10^{11} NPS/ml, although the injection amount was similar, $\sim$0.1–0.4 ml. The laser spot size was also not consistent from one experiment to another. Another variation is the laser radiance incident on the tumor surface, between 2 W/cm^2 and 50 W/cm^2. The large variations in the treatment protocols may suggest variations in tumor sizes, nanoshell/nanorod concentration in the tumors, its interaction with the laser light, and local blood perfusion rate in the tumors. The combinations of the nanostructure concentration, laser radiance, laser spot size, and heating time of all the previous studies did not always provide an intuitive trend expected by clinicians. In the limited few studies using direct nanoshell/nanorod injection to tumors, none of them have evaluated how the injec-

tion parameters such as injection amount, nanofluid concentration, and injection rate affect the nanostructure deposition and the resulting temperature elevations in the tumor.

3.5 Nanostructure Distribution in Tumors. Previous investigations have demonstrated that particle size, particle coating, and magnetic field strength and frequency or laser wavelength determine its heating generation capacity. However, once the nanoparticles/nanoshells are manufactured, the spatial distribution of the nanostructures dispersed in tissue dominates the spatial temperature elevation during heating. Therefore, understanding the distribution of nanostructures in tumors is critical in developing theoretical models to predict temperature distribution in tumors during hyperthermia treatment. An accurate description of the nanostructure distribution will greatly enhance the simulation accuracy of the heat transfer process in tumors, which is crucial in generating an optimal temperature distribution that can prevent the occurrence of heating underdosage in the tumor and overheating in the healthy tissue.

Delivery of magnetic nanoparticles or gold nanoshells/nanorods is typically performed via systemic (venous) injection of dispersed nanostructures in a biocompatible solution. Despite the small size of the nanostructures and the leaky nature of tumor vasculature, the accumulation of the nanostructures in a tumor is passive. Experiments have been performed in mice to demonstrate that it takes more than 6–10 h to gather all the nanoshells in the tumor site [109]. However, the coating on the nanoshells allows enhanced extravascular transport through the interaction between the coated receptor ligands on the nanoshells and tumor cell surface receptors [101]. For example, a newly developed molecular coupling agent is used to target epidermal growth factor receptor in cells [100,101]. The selective nature of the coating also allows minimal nanoshell accumulation in other organs or structures in the body. It will take a couple of days before the nanoshells are scavenged by the liver and spleen of the body [97,105].

The major challenge is to achieve a desired distribution of nanostructure in the tumor. Since the accumulation is passive, it is not clear how dispersed the nanostructures are after a systemic injection. Previous experimental data have suggested that the particle concentration is not uniform in tissue [81]. The concentration of nanostructures in tumors may vary from one region to another due to the variations in the permeability of the vasculature and local blood perfusion rate. In systemic delivery, it is difficult to deliver nanostructures to the necrotic tumor core region, which often survives with little blood supply. However, the tumor core has contributed to cancer recurrence after treatment since neither drug nor thermal agents are often delivered there to eradicate the tumor core. A recent study proposed a "Trojan" approach [110] to deliver nanoshells to the stubborn tumor core using elaborate biochemical procedures. For a tumor with a poor vascular supply, delivering nanostructure would take a long time for the passive accumulation. On the other hand, direct injection of nanostructures to tumors may be a feasible and practical approach. A very small amount of the carrier fluid containing nanoparticles or nanoshells can be directly injected into the tumor center. Rather than guessing where the nanostructures are placed and testing how long it takes for the nanostructures to be cleared from the bloodstream, it is expected that the nanostructure will be dispersed in the vicinity of the injection site. Temperature elevations in tumors are the direct result of the concentrated energy generation by the localized nanostructures as well as heat conduction from the injection sites.

Experimental observations of nanostructure distribution in tumors can be obtained following the approaches in the past in drug delivery. Nanostructures used in hyperthermia cancer treatment have a similar size range as the hydrodynamic radius of macromolecules in the drug delivery studies. For example, 2 MDa dextrans have a molecular size equivalent to a hydrodynamic radius of 25 nm [111]. Therefore, some of the previous animal experimental measurements of large molecular drug transport in cancer treatment may be applicable to the transport properties of the nanostructures in tumors. It was demonstrated in previous studies that the effective interstitial diffusion coefficient of drugs in tumors decreases as the drug molecule increases [112,113]. In addition, those experimental studies have illustrated a correlation between high levels of collagen type I and hindrance to diffusion when large drug molecules are involved [113]. Typical experimental approaches of evaluating drug/nanostructure distribution in tumors utilize fluorescently labeled drug molecules in implanted tumors in mice [112–114]. Due to the penetration limitation of confocal microscopy ($\sim$200 μm in depth) and other optical methods, drug transport in the interstitial space in tumors is evaluated via a 2D cranial or dorsal window chamber tumor preparation [111]. The complicated heterogeneous 3D tumor structure may not be well represented in the 2D tumor preparations, and the 3D drug transport process is often not completely captured by those approaches.

Earlier studies of the 3D nanostructure dispersion were performed in semitransparent gel, where the brown or black color of the nanofluid from the color of the gel can be used to track the nanofluid spreading during injections. It has been shown that the nanoparticles were confined in the vicinity of the injection site and that particle deposition was greatly affected by the injection rate and amount [81,82]. Although the tissue equivalent gels cannot completely mimic the real biological tissue, those gel studies have demonstrated that implementing a very slow injection rate ($\sim \mu$l/min) is critical to have controlled and repeatable nanoparticle concentration distributions. However, detailed nanoparticle deposition in the gel is difficult to quantify only based on the photo image of the gel.

Since tissue is opaque, 3D nanostructure distribution in tumors is usually unavailable. Recently, micro-CT imaging technique has been proposed as a noninvasive and nondestructive method for investigating nanoparticle distribution in tumors. Although micro-CT does not allow direct visualization of individual nanoparticles, the accumulation of nanoparticles in tissue would result in a region with a much higher density than the rest of the tissue, and the density variations can be detected by the micro-CT system [115,116]. A recent study has illustrated the feasibility of imaging and quantifying detailed 3D magnetic nanoparticle distribution in both gels and tumors [115]. In principle, different micro-CT pixel index numbers should represent the local nanoparticle concentration. For a high resolution micro-CT, the pixel size can be as small as several micrometers. A fast injection typically results in crack formation and uniform nanoparticle concentration surrounding the injection site in gels. However, nanoparticle diffusion from the injection site to the gel periphery is evident in the obtained micro-CT images, and an exponentially decaying nanoparticle distribution is observed. Heating experiments were performed later to confirm the linear correlation between the measured micro-CT pixel index number (0–256) and the generated local SAR value (W/kg) [115].

Similar experiments were also performed to image nanoparticle distribution in PC3 xenograft tumors implanted in Balbc/c Nu/Nu male mice [117]. Each mouse was inoculated on both flanks with 10^7 PC3 human prostate cancer cells. 0.1 ml water based ferrofluid was injected into one tumor at an injection rate of 5 μl/min. The tumor was subject to an alternating magnetic field (183 kHz), and its temperatures were elevated above 50°C for 15 min. After the heating experiment, the other tumor was injected the same amount of the ferrofluid at the same injection rate. Both tumors were then dissected from the mouse and loaded in the micro-CT system for X-ray scan. Figure 2 shows the nanoparticle concentration distribution illustrated by the light colors in the images. It appears that the nanoparticles were confined to the injection site, and they formed a regular shape after the injection. However, with heating, the nanoparticle distribution pattern looks different. The region occupied by the nanoparticles was quite irregular after the heating. The heating seems to cause the nanoparticles to move to

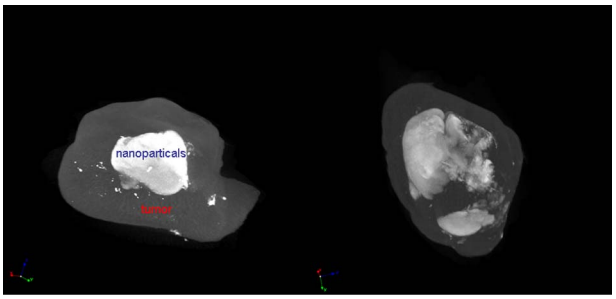

Fig. 2 Micro-CT images of nanoparticle deposition (bright color) in two tumors (dark color): (*a*) without heating and (*b*) after heating

the peripheral regions. However, more quantified micro-CT image analyses of the nanoparticle spreading in tumors are still needed. Since temperature elevations in tumors should be directly related to the local volumetric heat generation rate distribution, nanoparticle spreading more to the peripheral tumor regions favors a more uniform temperature elevation in tumors.

Nanostructure distribution in tissue can also be indirectly determined via measured temperature distributions in tissue. Based on the heat conduction equation, if the initial heat conduction can be neglected, the local volumetric heat generation rate or SAR can be measured by the initial temperature rise slope after the heating is turned on,

$$\mathrm{SAR} = \rho C \left.\frac{\partial T}{\partial t}\right|_{t=0} \tag{1}$$

where ρ is the tissue density, C is the specific heat, T is the tissue temperatures measured, and $t=0$ represents the initial time instance when the heating is turned on (electromagnetic field, laser, etc.). Several temperature sensors can be inserted into the tissue at various locations to obtain temperature rise curves at individual tissue locations. Typically, if the initial heat conduction in the tissue can be neglected, the measured temperatures should increase linearly once heating is turned on. After approximately 30 s, the temperature rise plot becomes curved, suggesting that heat conduction is no longer negligible. The slope in Eq. (1) is obtained by the measured temperature within the duration when the plot is still linear. After the experiment, the loose SAR values at all measuring sites are represented by an analytical expression reflecting the physical features of the energy generation patterns [68]. One of the limitations of this approach is the requirement of negligible heat conduction, which is difficult to satisfy in in vivo animal experiments. Considering the accuracy of the proposed analytical expression of the SAR, one also needs to place several temperature sensors in the tissue region where energy is generated. However, it is a challenge when the generated energy is concentrated in a small region. Nevertheless, this approach, although simple, has been used by researchers to determine the spatial distribution of nanoparticle generated SAR in tissue equivalent phantom gels [81]. In recent years, infrared thermography has been proposed to measure the temperature elevations in tissue during laser photothermal therapy. The high resolution infrared thermography technique is noninvasive without the need of placing any temperature sensors in tissue [107]. It is still difficult to quantify SAR inside the tissue using infrared thermography capable of only measuring surface temperatures.

In experimental studies using animal models, temperature elevations in tumors and tissue can be measured directly. The advancement in computational resources has allowed an accurate representation of the tumor and its surrounding tissue in numerical simulation softwares. Therefore, the measured temperature rises at individual tumor/tissue locations can extract the SAR distribution in tissue using inverse heat transfer analyses. An expression of the SAR distribution is proposed with several adjustable parameters. The temperature distribution in the tissue can then be simulated using computational software packages. Based on well established inverse heat transfer techniques, the parameters are adjusted to minimize a defined objective function representing deviations of the theoretical predictions from the experimentally measured temperatures. In an in vivo experiment using rats, magnetic nanoparticle generated SAR distribution is proposed as a simple Gaussian expression to mimic the nanoparticle deposition in tissue during direct intramuscular injection [82]. The extracted Gaussian expressions for different injection amounts have suggested a more concentrated nanoparticle deposition to the injection site when the injection amount is bigger. The observation is consistent with previous experiments by Prabhu et al. in drug delivery in the brain [118]. It is speculated that the earlier nanoparticle deposition on the solid cellular matrix of the tissue impedes the convection and diffusion by increasing the tissue hydraulic resistance. Therefore, additional nanoparticles injected later will deposit and accumulate close to the injection site. As one may see, the approach using inverse heat transfer analyses relies on the accuracy of the proposed SAR expression, as well as on the certainty of the tissue locations of the temperature sensors.

Theoretical models have been developed extensively to understand drug distribution in systemic or local drug delivery to tumors. The classic theory of colloidal particle infiltration through porous media [119,120] suggests that penetration of colloidal particles in porous structures is dependent on the properties of the particles, the velocity field, the physical-chemical properties of the solution, and the microstructure of the medium. Similarly, during the injection process of nanofluids, the penetration of nanostructures in the extracellular space of tissue is determined by the complex processes including diffusion and convection of carrier solution in porous tissue, particle transport in solution, particle agglomeration, deposition of particles on the tissue structure, and particle intake by cells and circulation. Significant research efforts have been focused on the migration of drugs in the extracellular space of tissue by conceptualizing biological tissue as a porous medium [121,122]. Conclusions derived from these studies have provided insights in the transport behavior of nanoparticles in tissue during injection processes.

The delivery of large therapeutic agents such as antibodies and nucleotides by pressure-driven intratumoral infusion has been extensively studied in the past decade [123–127]. However, the existing theory is not readily applicable to nanoparticles because the small size of the particles results in strong surface interactions that could lead to particle deposition on the cell surface. The deposition is dependent on many factors, including local fluid velocity, particle size, particle properties, surface properties and structure of the medium, and physicochemical properties of the aqueous environment. Recently, the approach of multiscale modeling, consisting of multiple components dealing with different length scales, has been utilized to provide a precise understanding of nanoparticle deposition in tissue. This approach is illustrated in a recently published research [128], where a microscale nanoparticle trajectory tracking model and a macroscale transport model in porous media are developed. In the trajectory tracking model, magnetic nanoparticles are modeled as individual entities. Their motion or trajectories in a unit cell structure of a porous medium are determined by the local velocity field in the carrier fluid, as well as the combined forces acting on the particle, including van der Waals attractive force, electrostatic double layer force, drag and lift force, buoyancy force, and Brownian motion. The simulation of the nanoparticle deposition on the solid matrix is then substituted into the macroscale transport model in porous media where fluid convection in the interstitial tissue space, diffusion of nanoparticle from a high concentrated region to a low concentrated one, and nanoparticle deposition rate on the solid matrix are considered. The microscale particle tracking model is important to

the macroscale model since the nanoparticle deposition on the solid structure reduces the nanoparticle concentration in the interstitial fluid, therefore limiting the penetration depth of the nanoparticles in tissue. Overall, the multiscale model has been shown to be in good agreement with experimental observations. It has greatly improved the simulation accuracy of nanoparticle transport in tissue. Further, modeling all the forces acting on individual nanoparticles is crucial to understanding contributions of various physical mechanisms to the motion of the particles. For example, the approach can be modified to model hydrodynamic interactions among particles, injection induced tissue deformation, and particle agglomeration during injection processes.

The knowledge and understanding of nanostructure transport can be applied to the study of nanotoxicology, which addresses the toxicity of nanomaterials to the human health. Nanomaterials may act upon living cells at the nanometer level, resulting in not only biologically desirable outcomes, but also undesirable effects such as inflammation and pro-oxidization. Nanomaterial exposure resulting from inhalation, dermal contact, or ingestion poses potential risks to the human health. Typically, the prediction of nanomaterial transport in the human body is an essential component in risk assessments; therefore, an investigative study must be undertaken to form the regulations for a safe research practice. Currently, one of the main obstacles toward a sound risk assessment is the uncertainty of the interaction between engineered materials and biological systems. Therefore, the new advancements in nanostructure transport in tumors can be extended to provide a fundamental understanding of the deposition of other nanomaterials in the human body through different routes as well as their responses to internal or external stimulations. Another potential field is targeted drug delivery using nanocarriers. The new imaging techniques and approaches of multiscale modeling can be applied to study nanocarrier extravasation from blood stream to tissue interstitial as well as later migration of therapeutic agents in the extracellular space of tissue. In addition to the already enlarged vascular permeability in tumors due to tumor's irregular and loose structure of neoplastic endothelium, heating would increase the leakage of nanocarriers to the interstitial space. Mild hyperthermia has been shown to also enhance cancer cell sensitivity to chemotherapy or radiation. Therefore, hyperthermia could be used as an adjuvant with those therapies to improve delivery of therapeutic agents and efficacy of those methods.

4 Conclusion Remarks

This review describes current advancements in biotransport and its clinical applications in two research fields. Despite its limitations, the Pennes bioheat equation is still used extensively in biotransport for modeling tissue temperature distribution during thermal treatments. Bioengineers have greatly improved their ability of modeling temperature fields in tissue with high precision for treatment planning with the advancements in computational resources and newly developed imaging tools, which allow an accurate description of the tissue geometry and heating source/sink distribution. This will greatly enhance the simulation accuracy of heat and mass transfer processes in tissue, which are critical for generating an optimal temperature distribution to achieve the clinical objectives. The challenges facing engineers in inducing fast brain hypothermia to brain injury patients are to identify noninvasive or minimally invasive technologies and devices, which are safe and effective and can be adapted to routine clinical treatment procedures. Hyperthermia treatments using newly developed nanostructures have the advantage over traditional heating approaches via providing confined heat generation in the targeted tumor region. High resolution imaging systems and multiscale modeling have tremendous potential for gaining insight into contributions of various transport mechanisms in nanostructure transport and distribution in tumors during both hyperthermia treatments and therapeutic agent delivery to the targeted tissue region.

Acknowledgment

This research was supported by NSF Grant Nos. CBET-0828728 and CBET-0821236 and a research grant from the University of Maryland Baltimore County (UMBC) Research Seed Funding Initiative.

References

[1] Pennes, H. H., 1948, "Analysis of Tissue and Arterial Blood Temperatures in the Resting Human Forearm," J. Appl. Physiol., **1**, pp. 93–122.

[2] Chato, J., 1980, "Heat Transfer to Blood Vessels," ASME J. Biomech. Eng., **102**, pp. 110–118.

[3] Chen, M. M., and Holmes, K. R., 1980, "Microvascular Contributions to Tissue Heat Transfer," Ann. N.Y. Acad. Sci., **335**, pp. 137–150.

[4] Weinbaum, S., Jiji, L. M., and Lemons, D. E., 1984, "Theory and Experiment for the Effect of Vascular Microstructure on Surface Tissue Heat Transfer—Part I: Anatomical Foundation and Model Conceptualization," ASME J. Biomech. Eng., **106**, pp. 321–330.

[5] Crezee, J., and Lagendijk, J. J. W., 1990, "Experimental Verification of Bioheat Transfer Theories: Measurement of Temperature Profiles around Large Artificial Vessels in Perfused Tissue," Phys. Med. Biol., **35**(7), pp. 905–923.

[6] He, Q., Zhu, L., Weinbaum, S., and Lemons, D. E., 2002, "Experimental Measurements of Temperature Variations Along Paired Vessels From 200 to 1000 μm in Diameter in Rat Hind Leg," J. Biomed. Eng., **124**, pp. 656–661.

[7] He, Q., Zhu, L., and Weinbaum, S., 2003, "Effect of Blood Flow on Thermal Equilibration and Venous Rewarming," Ann. Biomed. Eng., **31**, pp. 659–666.

[8] Lemons, D. E., Chien, S., Crawshaw, L. I., Weinbaum, S., and Jiji, L. M., 1987, "The Significance of Vessel Size and Type in Vascular Heat Transfer," Am. J. Physiol., **253**, pp. R128–R135.

[9] Song, J., Xu, L. X., Lemons, D. E., and Weinbaum, S., 1999, "Microvascular Thermal Equilibration in Rat Spinotrapezius Muscle," Ann. Biomed. Eng., **27**(1), pp. 56–66.

[10] Zhu, M., Weinbaum, S., and Lemons, D. E., 1988, "On the Generalization of the Weinbaun-Jiji Equation to Microvessels of Unequal Size: The Relation Between the Near Field and Local Average Tissue Temperature," ASME J. Biomech. Eng., **110**, pp. 74–81.

[11] Baish, J. W., 1994, "Formulation of a Statistical Model of Heat Transfer in Perfused Tissue," ASME J. Biomech. Eng., **116**, pp. 521–527.

[12] Weinbaum, S., and Jiji, L. M., 1985, "A New Simplified Bioheat Equation for the Effect of Blood Flow on Local Average Tissue Temperature," ASME J. Biomech. Eng., **107**, pp. 131–139.

[13] Weinbaum, S., Xu, L. X., Zhu, L., and Ekpene, A., 1997, "A New Fundamental Bioheat Equation for Muscle Tissue: Part I—Blood Perfusion Term," ASME J. Biomech. Eng., **119**, pp. 278–288.

[14] Zhu, L., Xu, L. X., He, Q., and Weinbaum, S., 2002, "A New Fundamental Bioheat Equation for Muscle Tissue, Part II: Temperature of SAV Vessels," ASME J. Biomech. Eng., **124**, pp. 121–132.

[15] Nakayama, A., and Kuwahara, F., 2008, "A General Bioheat Transfer Model Based on the Theory of Porous Media," Int. J. Heat Mass Transfer, **51**, pp. 3190–3199.

[16] Shrivastava, D., and Vaughan, J. T., 2009, "A Generic Bioheat Transfer Thermal Model for a Perfused Tissue," ASME J. Biomech. Eng., **131**, p. 074506.

[17] Bischof, J. C., 2000, "Quantitative Measurement and Prediction of Biophysical Response During Freezing in Tissue," Annu. Rev. Biomed. Eng., **2**, pp. 257–288.

[18] Diller, K., 1992, "Modeling of Bioheat Transfer Processes at High and Low Temperatures," *Bioengineering Heat Transfer: Advances in Heat Transfer*, Vol. 22, Y. I. Cho, ed., Academic Press, San Diego, CA, pp. 157–357.

[19] Diller, K., 2006, "Stress Protein Expression Kinetics," Annu. Rev. Biomed. Eng., **8**, pp. 403–424.

[20] Welch, A. J., and van Gemert, M. J. C., 1995, *Optical-Thermal Response of Laser-Irradiated Tissue*, Plenum, New York.

[21] Bigelow, W. G., Callaghan, J. C., and Hopps, J. A., 1950, "General Hypothermia for Experimental Intracardiac Surgery: The Use of Electrophrenic Respirations, an Artificial Pacemaker for Cardiac Standstill, and Radio-Frequency Rewarming in General Hypothermia," Ann. Surg., **132**, pp. 531–539.

[22] Drake, C. G., and Jory, T. A., 1962, "Hypothermia in the Treatment of Critical Head Injury," Can. Med. Assoc. J., **87**, pp. 887–891.

[23] Lazorthes, G., and Campan, L., 1958, "Hypothermia in the Treatment of Craniocerebral Traumatism," J. Neurosurg., **15**, pp. 162–167.

[24] Rosomoff, H. L., 2004, "Historical Review of the Development of Brain Hypothermia," *Hypothermia for Acute Brain Damage: Pathomechanism and Practical Aspects*, N. Hayashi, R. Bullock, D. W. Dietrich, T. Maekawa, and A. Tamura, eds., Springer, New York, pp. 3–16.

[25] Safar, P., 2002, "Cerebral Resuscitation From Temporary Complete Global Brain Ischemia," *Cerebral Blood Flow: Mechanisms of Ischemia, Diagnosis and Therapy*, M. R. Pinsky, ed., Springer-Verlag, Berlin, pp. 106–136.

[26] van der Worp, H. B., Sena, E. S., Donnan, G. A., Howells, D. W., and Macleod, M. R., 2007, "Hypothermia in Animal Models of Acute Ischaemic Stroke: A Systematic Review and Meta-Analysis," Brain, **130**, pp. 3063–3074.

[27] Dietrich, W. D., Prado, R., Halley, M., and Watson, B. D., 1993, "Microvascular and Neuronal Consequences of Common Carotid Artery Thrombosis and Platelet Embolization in Rats," J. Neuropathol. Exp. Neurol., **52**(4), pp. 351–360.

[28] Welsh, F. A., Sims, R. E., and Harris, V. A., 1990, "Mild Hypothermia Pre-

vents Ischemic Injury in Gerbil Hippocampus," J. Cereb. Blood Flow Metab., **10**, pp. 557–563.
[29] Barres, A. B., and Raff, M. C., 1993, "Proliferation of Oligodendrocyte Precursor Cells Depends on Electrical Activities in Axons," Nature (London), **361**, pp. 258–260.
[30] Shi, J., Marinovich, A., and Barres, B. A., 1998, "Purification and Characterization of Adult Oligodendrocyte Precursor Cells From the Rat Optic Nerve," J. Neurosci., **18**, pp. 4627–4636.
[31] White, L. J., and Dressendorfer, R. H., 2004, "Exercise and Multiple Sclerosis," Sports Med., **34**(15), pp. 1077–1100.
[32] Grahn, D. A., Brock-Utne, J. G., Watenpaugh, D. E., and Heller, H. C., 1998, "Recovery From Mild Hypothermia Can Be Accelerated by Mechanically Distending Blood Vessels in the Hand," J. Appl. Physiol., **85**, pp. 1643–1648.
[33] Grahn, D. A., Cao, V. H., and Heller, H. C., 2005, "Heat Extraction Through the Palm of One Hand Improves Aerobic Exercise Endurance in a Hot Environment," J. Appl. Physiol., **99**(3), pp. 972–978.
[34] Grahn, D. A., Dillon, J. L., and Heller, H. C., 2009, "Heat Loss Through the Glabrous Skin Surfaces of Heavily Insulated, Heat-Stressed Individuals," ASME J. Biomech. Eng., **131**, p. 071005.
[35] Kammersgaard, L. P., Rasmussen, B. H., Jorgensen, H. S., Reith, J., Weber, U., and Olsen, T. S., 2000, "Feasibility and Safety of Inducing Modest Hypothermia in Awake Patients With Acute Stroke Through Surface Cooling: A Case-Control Study," Stroke, **31**, pp. 2251–2256.
[36] Olsen, T. S., Weber, U. J., and Kammersgaard, L. P., 2003, "Therapeutic Hypothermia for Acute Stroke," Lancet Neurol., **2**, pp. 410–416.
[37] Schwab, S., Spranger, M., Aschoff, A., Steiner, T., and Hacke, W., 1997, "Brain Temperature Monitoring and Modulation in Patients With Severe MCA Infarction," Neurology, **48**, pp. 762–767.
[38] Holzer, M., Müllner, M., Sterz, F., Robak, O., Kliegel, A., Losert, H., Sodeck, G., Uray, T., Zeiner, A., and Laggner, A. N., 2006, "Efficacy and Safety of Endovascular Cooling After Cardiac Arrest: Cohort Study and Bayesian Approach," Stroke, **37**, pp. 1792–1797.
[39] Keller, E., Imhof, H.-G., Gasser, S., Terzic, A., and Yonekawa, Y., 2003, "Endovascular Cooling With Heat Exchange Catheters: A New Method to Induce and Maintain Hypothermia," Intensive Care Med., **29**, pp. 939–943.
[40] Lyden, P. D., Allgren, R. L., Ng, K., Akins, P., Meyer, B., Al-Sanani, F., Lutsep, H., Dobak, J., Matsubara, B. S., and Zivin, J., 2005, "Intravascular Cooling in the Treatment of Stroke (ICTuS): Early Clinical Experience," J. Stroke Cerebrovasc. Dis., **14**(3), pp. 107–114.
[41] Bakken, H. E., Kawasaki, H., Oya, H., Greenlee, J. D. W., and Howard, M. A., 2003, "A Device for Cooling Localized Regions of Human Cerebral Cortex," J. Neurosurg., **99**, pp. 604–608.
[42] Diao, C., Zhu, L., and Wang, H., 2003, "Cooling and Rewarming for Brain Ischemia or Injury: Theoretical Analysis," Ann. Biomed. Eng., **31**, pp. 346–353.
[43] Ku, Y., Montgomery, L. D., and Webbon, B., 1996, "Hemodynamic and Thermal Responses to Head and Neck Cooling in Men and Woman," Am. J. Phys. Med. Rehabil., **75**, pp. 443–450.
[44] Laptook, A. R., Shalak, L., and Corbett, R. J. T., 2001, "Differences in Brain Temperature and Cerebral Blood Flow During Selective Head Versus Whole-Body Cooling," Pediatrics, **108**(5), pp. 1103–1110.
[45] Noguchi, Y., Nishio, S., Kawuchi, M., Asari, S., and Ohmoto, T., 2002, "A New Method of Inducing Selective Brain Hypothermia With Saline Perfusion Into the Subdural Space: Effects on Transient Cerebral Ischemia in Cats," Acta Med. Okayama, **56**, pp. 279–286.
[46] Zhu, L., and Rosengart, A. J., 2008, "Cooling Penetration Into Normal and Injured Brain via Intraparenchymal Brain Cooling Probe: Theoretical Analyses," Heat Transfer Eng., **29**(3), pp. 284–294.
[47] Ding, Y., Li, J., Luan, X., Lai, Q., McAllister, J. P., Phillis, J. W., Clark, J. C., Guthikonda, M., and Diaz, F. G., 2004, "Local Saline Infusion Into Ischemic Territory Induces Regional Brain Cooling and Neuroprotection in Rats With Transient Middle Cerebral Artery Occlusion," Neurosurgery, **54**, pp. 956–965.
[48] Neimark, M. A., Konstas, A., Choi, J. H., Laine, A. F., and Pile-Spellman, J., 2008, "Brain Cooling Maintenance With Cooling Cap Following Induction With Intracarotid Cold Saline Infusion: A Quantitative Model," J. Theor. Biol., **253**(2), pp. 333–344.
[49] Wang, Y., and Zhu, L., 2007, "Selective Brain Hypothermia Induced by an Interstitial Cooling Device in Human Neck: Theoretical Analyses," Eur. J. Appl. Physiol., **101**, pp. 31–40.
[50] Wang, Y., Zhu, L., and Rosengart, A. J., 2008, "Targeted Brain Hypothermia Induced by an Interstitial Cooling Device in the Rat Neck: Experimental Study and Model Validation," Int. J. Heat Mass Transfer, **51**, pp. 5662–5670.
[51] Wei, G., Hartings, J. A., Yang, X., Tortella, F. C., and Lu, X.-C. M., 2008, "Extraluminal Cooling of Bilateral Common Carotid Arteries as a Method to Achieve Selective Brain Cooling for Neuroprotection," J. Neurotrauma, **25**, pp. 549–559.
[52] Attaluri, A., Huang, Z., and Zhu, L., 2010, "Evaluation of an Interstitial Cooling Device for Carotid Arterial Cooling Using Tissue Equivalent Gel Phantom," J. Thermodynamic Sciences and Engineering Applications, **2**, p. 011007.
[53] Bommadevara, M., and Zhu, L., 2002, "Temperature Difference Between the Body Core and Arterial Blood Supplied to the Brain During Hyperthermia or Hypothermia in Humans," Biomech. Model. Mechanobiol., **1**(2), pp. 137–149.
[54] Eginton, M. L., 2007, "Evaluation of the Effectiveness of a Commercial Cooling Collar in Reducing Body Temperature During Heat Stress: Theoretical Modeling of Body Temperature Distribution," MS thesis, University of Maryland, Baltimore, MD, pp. 1–55.
[55] Georgiadis, D., Schwarz, S., Kollmar, R., and Schwab, S., 2001, "Endovascular Cooling for Moderate Hypothermia in Patients With Acute Stroke: First Results of a Novel Approach," Stroke, **32**, pp. 2550–2553.
[56] Dennis, B. H., Eberhart, R. C., Dulikravich, G. S., and Radons, S. W., 2003, "Finite Element Simulation of Cooling of Realistic 3-D Human Head and Neck," ASME J. Biomech. Eng., **125**, pp. 832–840.
[57] Janssen, F. E. M., van Leeuwen, G. M. J., and van Steenhoven, A. A., 2005, "Modeling of Temperature and Perfusion During Scalp Cooling," Phys. Med. Biol., **50**(17), pp. 4065–4073.
[58] Ley, O., and Bayazitoglu, Y., 2003, "Effect of Physiology on the Temperature Distribution of a Layered Head With External Convection," Int. J. Heat Mass Transfer, **46**(17), pp. 3233–3241.
[59] van Leeuwen, G. M. J., Hand, J. W., Lagendijk, J. W., Azzopardi, D. V., and Edwards, A. D., 2000, "Numerical Modeling of Temperature Distributions Within the Neonatal Head," Pediatr. Res., **48**, pp. 351–356.
[60] Zhu, L., Schappeler, T., Cordero-Tumangday, C., and Rosengart, A. J., 2009, "Thermal Interactions Between Blood and Tissue: Development of a Theoretical Approach in Predicting Body Temperature During Blood Cooling/Rewarming," *Advances in Numerical Heat Transfer*, Vol. 3, W. J. Minkowycz and E. M. Sparrow, eds., CRC, Boca Raton, FL, pp. 197–219.
[61] Diao, C., and Zhu, L., 2006, "Temperature Distribution and Blood Flow Response in Rat Brain During Selective Brain Cooling," Med. Phys., **33**(7), pp. 2565–2573.
[62] Bering, E., 1961, "Effect of Body Temperature Change on Cerebral Oxygen Consumption of the Intact Monkey," Am. J. Physiol., **200**, pp. 417–419.
[63] Scheinman, M. M., Morady, F., Hess, D. S., and Gonzalez, R., 1982, "Catheter-Induced Ablation of the Atrioventricular Junction to Control Refractory Supraventricular Arrhythmias," JAMA, J. Am. Med. Assoc., **248**, pp. 851–855.
[64] Nath, S., and Haines, D. E., 1995, "Biophysics and Pathology of Catheter Energy Delivery System," Prog. Cardiovasc. Dis., **37**(4), pp. 185–204.
[65] Patel, N. K., Heywood, P., O'Sullivan, K., McCarter, R., Love, S., and Gill, S. S., 2003, "Unilateral Subthalamotomy in the Treatment of Parkinson's Disease," Brain, **126**, pp. 1136–1145.
[66] Wonnell, T. L., Stauffer, P. R., and Langberg, J. J., 1992, "Evaluation of Microwave and Radio Frequency Catheter Ablation in a Myocardium-Equivalent Phantom Model," IEEE Trans. Biomed. Eng., **39**, pp. 1086–1095.
[67] Zhu, L., and Xu, L. X., 1999, "Evaluation of the Effectiveness of Transurethral Radio Frequency Hyperthermia in the Canine Prostate: Temperature Distribution Analysis," ASME J. Biomech. Eng., **121**, pp. 584–590.
[68] Zhu, L., Xu, L. X., and Chencinski, N., 1998, "Quantification of the 3-D Electromagnetic Power Absorption Rate in Tissue During Transurethral Prostatic Microwave Thermotherapy Using Heat Transfer Model," IEEE Trans. Biomed. Eng., **45**(9), pp. 1163–1172.
[69] Flower, R. W., 2002, "Optimizing Treatment of Choroidal Neovascularization Feeder Vessels Associated With Age-Related Macular Degeneration," Am. J. Ophthalmol., **134**, pp. 228–239.
[70] Zhu, L., Banerjee, R. K., Salloum, M., Bachmann, A. J., and Flower, R. W., 2008, "Temperature Distribution During ICG Dye-Enhanced Laser Photocoagulation of Feeder Vessels in Treatment of AMD-Related Choroidal Neovascularization (CNV)," ASME J. Biomech. Eng., **130**(3), p. 031010.
[71] Jia, W., Aguilar, G., Verkruysse, W., Franco, W., and Nelson, J. S., 2006, "Improvement of Port Wine Stain Laser Therapy by Skin Preheating Prior to Cryogen Spray Cooling: A Numerical Simulation," Lasers Surg. Med., **38**, pp. 155–162.
[72] Huikeshoven, M., Koster, P. H., de Borgie, C. A., Beek, J. F., van Gemert, M. J., and van der Horst, C. M., 2007, "Redarkening of Port-Wine Stains 10 Years After Pulsed-Dye-Laser Treatment," N. Engl. J. Med., **356**(12), pp. 1235–1240.
[73] Jasim, Z. F., and Handley, J. M., 2007, "Treatment of Pulsed Dye Laser Resistant Port Wine Stain Birthmarks," J. Am. Acad. Dermatol., **57**(4), pp. 677–682.
[74] Izikson, L., Nelson, J. S., and Anderson, R. R., 2009, "Treatment of Hypertrophic and Resistant Port Wine Stains With a 755 nm Laser: A Case Series of 20 Patients," Lasers Surg. Med., **41**(6), pp. 427–432.
[75] Zhu, L., Tolba, M., Arola, D., Salloum, M., and Meza, F., 2009, "Evaluation of Effectiveness of Er,Cr:YSGG Laser for Root Canal Disinfection: Theoretical Simulation of Temperature Elevations in Root Dentin," ASME J. Biomech. Eng., **131**(7), p. 071004.
[76] Barberia, E., Maroto, M., Arenas, M., and Silva, C. C., 2008, "A Clinical Study of Caries Diagnosis With a Laser Fluorescence System," J. Am. Dent. Assoc., **139**, pp. 572–579.
[77] Chu, C. H., Lo, E. C. M., and You, D. S. H., 2010, "Clinical Diagnosis of Fissure Caries With Conventional and Laser-Induced Fluorescence Techniques," Lasers Med. Sci., **25**, pp. 355–362.
[78] Du, L., Zhou, J., Wang, X., Sheng, L., Wang, G., Xie, X., Xu, G., Zhao, L., Liao, Y., and Tang, J., 2009, "Effect of Local Hyperthermia Induced by Nanometer Magnetic Fluid on the Rabbit VX2 Liver Tumor Model," Prog. Nat. Sci., **19**(12), pp. 1705–1712.
[79] Gazeau, F., Lévy, M., and Wilhelm, C., 2008, "Optimizing Magnetic Nanoparticle Design for Nanothermotherapy," Nanomedicine, **3**(6), pp. 831–844.
[80] Jordan, A., Scholz, R., Wust, P., Fahling, H., and Felix, R., 1999, "Magnetic Fluid Hyperthermia (MFH): Cancer Treatment With AC Magnetic Field Induced Excitation of Biocompatible Superparamagnetic Nanoparticles," J. Magn. Magn. Mater., **201**, pp. 413–419.
[81] Salloum, M., Ma, R., Weeks, D., and Zhu, L., 2008, "Controlling Nanoparticle

Delivery in Magnetic Nanoparticle Hyperthermia for Cancer Treatment: Experimental Study in Agarose Gel," Int. J. Hyperthermia, **24**(4), pp. 337–345.
[82] Salloum, M., Ma, R., and Zhu, L., 2008, "An In-Vivo Experimental Study of Temperature Elevations in Animal Tissue During Magnetic Nanoparticle Hyperthermia," Int. J. Hyperthermia, **24**(7), pp. 589–601.
[83] Salloum, M., Ma, R., and Zhu, L., 2009, "Enhancement in Treatment Planning for Magnetic Nanoparticle Hyperthermia: Optimization of the Heat Absorption Pattern," Int. J. Hyperthermia, **25**(4), pp. 309–321.
[84] Skrabalak, S. E., Chen, J., Au, L., Lu, X., Li, X., and Xia, Y., 2007, "Gold Nanocages for Biomedical Applications," Adv. Mater., **19**, pp. 3177–3184.
[85] Gilchrist, R. K., Medal, R., Shorey, W. D., Hanselman, R. C., Parrott, J. C., and Taylor, C. B., 1957, "Selective Inductive Heating of Lymph Nodes," Ann. Surg., **146**, pp. 596–606.
[86] Hilger, I., Hergt, R., and Kaiser, W. A., 2005, "Towards Breast Cancer Treatment by Magnetic Heating," J. Magn. Magn. Mater., **293**, pp. 314–319.
[87] Moroz, P., Jones, S. K., and Gray, B. N., 2002, "Magnetically Mediated Hyperthermia: Current Status and Future Directions," Int. J. Hyperthermia, **18**(4), pp. 267–284.
[88] Hergt, R., and Andra, W., 1998, "Physical Limits of Hyperthermia Using Magnetite Fine Particles," IEEE Trans. Magn., **34**(5), pp. 3745–3754.
[89] Rosensweig, R. E., 2002, "Heating Magnetic Fluid With Alternating Magnetic Field," J. Magn. Magn. Mater., **252**, pp. 370–374.
[90] Hergt, R., Hiergeist, R., Zeisberger, M., Glockl, G., Weitschies, W., Ramirez, L. P., Hilger, I., and Kaiser, W. A., 2004, "Enhancement of AC-Losses of Magnetic Nanoparticles for Heating Applications," J. Magn. Magn. Mater., **280**, pp. 358–368.
[91] Hilger, I., Andra, W., Hergt, R., Hiergeist, R., Schubert, H., and Kaiser, W. A., 2001, "Electromagnetic Heating of Breast Tumors in Interventional Radiology: In Vitro and in Vivo Studies in Human Cadavers and Mice," Radiology, **218**(2), pp. 570–575.
[92] Johannsen, M., Jordan, A., Scholz, R., Koch, M., Lein, M., Deger, S., Roigas, J., Jung, K., and Loening, S., 2004, "Evaluation of Magnetic Fluid Hyperthermia in a Standard Rat Model of Prostate Cancer," J. Endourol, **18**(5), pp. 495–500.
[93] Johannsen, M., Thiesen, B., Jordan, A., Taymoorian, K., Gneveckow, U., Waldofner, N., Scholz, R., Koch, M., Lein, M., and Jung, K., 2005, "Magnetic Fluid Hyperthermia (MFH) Reduces Prostate Cancer Growth in the Orthotopic Dunning R3327 Rat Model," Prostate, **64**, pp. 283–292.
[94] Jordan, A., Scholz, R., Maier-Hauff, K., van Landeghem, F. K., Waldoefner, N., Teichgraeber, U., Pinkernelle, J., Bruhn, H., Neumann, F., Thiesen, B., von Deimling, A., and Felix, R., 2006, "The Effect of Thermotherapy Using Magnetic Nanoparticles on Rat Malignant Glioma," J. Neuro-Oncol., **78**, pp. 7–14.
[95] Fortin, J. P., Gazeau, F., and Wilhelm, C., 2008, "Intracellular Heating of Living Cells Through Néel Relaxation of Magnetic Nanoparticles," Eur. Biophys. J., **37**(2), pp. 223–228.
[96] Averitt, R. D., Sarkar, D., and Halas, N. J., 1997, "Plasmon Resonance Shifts of Au-Coated Au_2S Nanoshells: Insight Into Multicomponent Nanoparticle Growth," Phys. Rev. Lett., **78**, pp. 4217–4220.
[97] Lal, S., Clare, S. E., and Halas, N. J., 2008, "Nanoshell-Enabled Photothermal Cancer Therapy: Impending Clinical Impact," Acc. Chem. Res., **41**(12), pp. 1842–1851.
[98] Bernardi, R. J., Lowery, A. R., Thompson, P. A., Blaney, S. M., and West, J. L., 2008, "Immunonanoshells for Targeted Photothermal Ablation in Medulloblastoma and Glioma: An In Vitro Evaluation Using Human Cell Lines," J. Neuro-Oncol., **86**, pp. 165–172.
[99] El-Sayed, I. H., Huang, X., and El-Sayed, M. A., 2006, "Selective Laser Photo-Thermal Therapy of Epithelial Carcinoma Using Anti-EGFR Antibody Conjugated Gold Nanoparticles," Cancer Lett., **239**, pp. 129–135.
[100] Gobin, A. M., Moon, J. J., and West, J. L., 2008, "EphrinAl-Targeted Nanoshells for Photothermal Ablation of Prostate Cancer Cells," Int. J. Nanomedicine, **3**(3), pp. 351–358.
[101] Melancon, M. P., Lu, W., Yang, Z., Zhang, R., Cheng, Z., Elliot, A. M., Stafford, J., Olson, T., Zhang, J. Z., and Li, C., 2008, "In Vitro and In Vivo Targeting of Hollow Gold Nanoshells Directed at Epidermal Growth Factor Receptor for Photothermal Ablation Therapy," Mol. Cancer Ther., **7**(6), pp. 1730–1739.
[102] Norman, R. S., Stone, J. W., Gole, A., Murphy, C. J., and Sabo-Attwood, T. L., 2008, "Targeted Photothermal Lysis of the Pathogenic Bacteria, Pseudomonas Aeruginosaa, With Gold Nanorods," Nano Lett., **8**(1), pp. 302–306.
[103] Whitney, J., Dorn, H., Rylander, C., Campbell, T., Geohegan, D., and Rylander, M. N., 2010, "Spatiotemporal Temperature and Cell Viability Measurement Following Laser Therapy in Combination With Carbon Nanohorns," *Proceedings of the Summer Bioengineering Engineering Conference*, Paper No. SBC2010-19619.
[104] O'Neal, D. P., Hirsch, L. R., Halas, N. J., Payne, J. D., and West, J. L., 2004, "Photo-Thermal Tumor Ablation in Mice Using Near Infrared-Absorbing Nanoparticles," Cancer Lett., **209**, pp. 171–176.
[105] Stern, J. M., Stanfield, J., Kabbani, W., Hsieh, J.-T., and Cadeddu, J. A., 2008, "Selective Prostate Cancer Thermal Ablation With Laser Activated Cold Nanoshells," J. Urol. (Baltimore), **179**, pp. 748–753.
[106] Hirsch, L. R., Stafford, R. J., Bankson, J. A., Sershen, S. R., Rivera, B., Price, R. E., Hazle, J. D., Halas, N. J., and West, J. L., 2003, "Nanoshell-Mediated Near-Infrared Thermal Therapy of Tumors Under Magnetic Resonance Guidance," Proc. Natl. Acad. Sci. U.S.A., **100**(23), pp. 13549–13554.
[107] Qin, Z., and Bischof, J. C., 2010, "One Dimensional Experimental Setup to Study the Heating of Nanoparticle Laden Systems," *Proceedings of the Summer Bioengineering Engineering Conference*, Paper No. SBC2010-19676.
[108] Elliott, A. M., Stafford, R. J., Schwartz, J., Wang, J., Shetty, A. M., Bourgoyne, C., O'Neal, P., and Hazle, J. D., 2007, "Laser-Induced Thermal Response and Characterization of Nanoparticles for Cancer Treatment Using Magnetic Resonance Thermal Imaging," Med. Phys., **34**, pp. 3102–3108.
[109] Xie, H., Gill-Sharp, K. L., and O'Neal, D. P., 2007, "Quantitative Estimation of Gold Nanoshell Concentrations in Whole Blood Using Dynamic Light Scattering," Nanomedicine, **3**, pp. 89–94.
[110] Choi, M. R., Stanton-Maxey, K. J., Stanley, J. K., Levin, C. S., Bardhan, R., Akin, D., Badve, S., Sturgis, J., Robinson, J. P., Bashir, R., Halas, N. J., and Clare, S. E., 2007, "A Cellular Trojan Horse for Delivery of Therapeutic Nanoparticles Into Tumors," Nano Lett., **7**, pp. 3759–3765.
[111] Dreher, M. R., Liu, W., Michelich, C. R., Dewhirst, M. W., Yuan, F., and Chilkoti, A., 2006, "Tumor Vascular Permeability, Accumulation, and Penetration of Macromolecular Drug Carriers," Int. J. Radiat. Oncol., Biol., Phys., **32**, pp. 1419–1423.
[112] Berk, D. A., Yuan, F., Leunig, M., and Jain, R. K., 1993, "Fluorescence Photobleaching With Spatial Fourier Analysis: Measurement of Diffusion in Light-Scattering Media," Biophys. J., **65**, pp. 2428–2436.
[113] Pluen, A., Boucher, Y., Ramanujan, S., McKee, T. D., Gohongi, R., DiTomaso, E., Brown, E. B., Izumi, Y., Campbell, R. B., Berk, D. A., and Jain, R. K., 2001, "Role of Tumor-Host Interactions in Interstitial Diffusion of Macromolecules: Cranial vs. Subcutaneous Tumors," Proc. Natl. Acad. Sci. U.S.A., **98**, pp. 4628–4633.
[114] Liu, P., Zhang, A., Xu, Y., and Xu, L. X., 2005, "Study of Non-Uniform Nanoparticle Liposome Extravasation in Tumor," Int. J. Hyperthermia, **21**, pp. 259–270.
[115] Attaluri, A., Ma, R., and Zhu, L., 2011, "Using MicroCT Imaging Technique to Quantify Heat Generation Distribution Induced by Magnetic Nanoparticles for Cancer Treatment," ASME J. Heat Transfer, **133**, p. 011003.
[116] von Maltzahn, G., Park, J.-H., Agrawal, A., Bandaru, N. K., Das, S. K., Sailor, M. J., and Bhatia, S. N., 2009, "Computationally Guided Photothermal Tumor Therapy Using Long-Circulating Gold Nanorod Antennas," Cancer Res., **69**, pp. 3892–3900.
[117] Attaluri, A., Ma, R., Qiu, Y., Li, W., and Zhu, L., "Nanoparticle Distribution and Temperature Elevations in Prostatic Tumors in Mice During Magnetic Nanoparticle Hyperthermia," Int. J. Hyperthermia, submitted.
[118] Prabhu, S. S., Broaddus, W. C., Gillies, G. T., Loudon, W. G., Chen, Z. J., and Smith, B., 1998, "Distribution of Macromolecular Dyes in Brain Using Positive Pressure Infusion: A Model for Direct Controlled Delivery of Therapeutic Agents," Surg. Neurol., **50**, pp. 367–375.
[119] Elimelech, M., and O'Melia, C. R., 1990, "Kinetics of Deposition of Colloidal Particles in Porous Media," Environ. Sci. Technol., **24**, pp. 1528–1536.
[120] Khaled, A. R. A., and Vafai, K., 2003, "The Role of Porous Media in Modeling Flow and Heat Transfer in Biological Tissues," Int. J. Heat Mass Transfer, **46**, pp. 4989–5003.
[121] Kim, A. S., and Yuan, R., 2005, "Hydrodynamics of an Ideal Aggregate With Quadratically Increasing Permeability," J. Colloid Interface Sci., **285**, pp. 627–633.
[122] Ramanujan, S., Pluen, A., McKee, T. D., Brown, E. B., Boucher, Y., and Jain, R. K., 2002, "Diffusion and Convection in Collagen Gels: Implications for Transport in the Tumor Interstitium," Biophys. J., **83**, pp. 1650–1660.
[123] Bobo, R. H., Laske, D. W., Akbasak, A., Morrison, P. F., Dedrick, R. L., and Oldfield, E. H., 1994, "Convection-Enhanced Delivery of Macromolecules in the Brain," Proc. Natl. Acad. Sci. U.S.A., **91**(6), pp. 2076–2080.
[124] Dillehay, L. E., 1997, "Decreasing Resistance During Fast Infusion of a Subcutaneous Tumor," Anticancer Res., **17**(1A), pp. 461–466.
[125] Jain, R. K., 1997, "Delivery of Molecular and Cellular Medicine to Solid Tumors," Adv. Drug Delivery Rev., **26**, pp. 71–90.
[126] McGuire, S., and Yuan, F., 2001, "Quantitative Analysis of Intratumoral Infusion of Color Molecules," Am. J. Physiol., **281**(2), pp. H715–H721.
[127] Wang, Y., Wang, H., Li, C. Y., and Yuan, F., 2006, "Effects of Rate, Volume, and Dose of Intratumoral Infusion on Virus Dissemination in Local Gene Delivery," Mol. Cancer Ther., **5**(2), pp. 362–366.
[128] Su, D., Ma, R., Salloum, M., and Zhu, L., 2010, "Multi-Scale Study of Nanoparticle Transport and Deposition in Tissues During an Injection Process," Med. Biol. Eng. Comput., **48**, pp. 853–863.